Fluorophosphates from Solid#State Synthesis and Electrochemical Ion Exchange: NaVPO 4 F or Na 3 V 2 (PO 4) 2 F 3 ?

Fluorophosphates from Solid-State Synthesis and Electrochemical Ion Exchange: $NaVPO_4F$ or $Na_3V_2(PO_4)_2F_3$?

Long Li[1,2], Youlong Xu[1,2,*], Xiaofei Sun[1,2], Rui Chang[2], Yuan Zhang[1,2], Xiaona Zhang[1,2], Ju Li[3,*]

[1]Electronic Materials Research Laboratory, Key Laboratory of the Ministry of Education & International Center for Dielectric Research, Xi'an Jiaotong University, Xi'an 710049 PR China

[2]Shaanxi Engineering Research Center of Advanced Energy Materials & Devices, Xi'an Jiaotong University, Xi'an, China

[3]Department of Nuclear Science and Engineering and Department of Materials Science and Engineering, Massachusetts Institute of Technology Cambridge, MA 02139

[*]*Corresponding author: ylxu@mail.xjtu.edu.cn* (Youlong Xu)

liju@mit.edu (Ju Li)

Abstract

Vanadium-based fluorophosphates are promising sodium-ion battery cathode materials. Different phases of $NaVPO_4F$ and $Na_3V_2(PO_4)_2F_3$ have been reported in the literature. However, our experiments suggest there could be confusions about the single-phase in solid-state synthesis. Here, systematic investigation of the mechanism underlying structural and compositional evolution of solid-state synthesis ($NaF:VPO_4$=1:1) is determined by in-situ and ex-situ X-ray diffraction and electrochemical measurements. Three reactions:

$3NaF+3VPO_4 \rightarrow Na_3V_2(PO_4)_2F_3+VPO_4$ (up to 500°C),

$Na_3V_2(PO_4)_2F_3+VPO_4 \rightarrow Na_3V_2(PO_4)_3+VF_3\uparrow$ (600 to 800 °C), and $2Na_3V_2(PO_4)_3 \rightarrow 2(VO)_2P_2O_7+Na_4P_2O_7$+amorphous products (above 800 °C), are validated by *in situ* XRD and thermogravimetric analysis/differential scanning calorimetry. None of our products are consistent with single-phase $NaVPO_4F$ at any temperature. We speculate that the assignments of *I4/mmm* and C_2/c $NaVPO_4F$ from solid-state synthesis are incorrect, which are instead multi-phase mixtures of Le Meins' $Na_3V_2(PO_4)_2F_3$, unreacted VPO_4 and hexagonal $Na_3V_2(PO_4)_3$. Liquid-electrolyte based electrochemical ion exchange of $LiVPO_4F$ produces a tavorite $NaVPO_4F$ structure, very different from Le Meins' family of $Na_3Al_2(PO_4)_2F_3$ polymorphs.

Keywords: volatile VF_3 gas, $Na_3V_2(PO_4)_3$, tavorite-type $NaVPO_4F$

Introduction

Sodium-ion batteries (SIBs) are promising alternatives to lithium-ion batteries (LIBs) for large-scale energy storage.[1] Due to the high operating voltage and thermal stability, vanadium-based fluorophosphates have aroused great interest as potential cathode materials for rechargeable SIBs.[1c, 2] Among these structures, $NaVPO_4F$ ($NaF:VPO_4$=1:1) and $Na_3V_2(PO_4)_2F_3$ ($NaF:VPO_4$=3:2) were first shown by Barker group in 2003 and 2006

respectively as reversible insertion hosts for SIBs.[3] Both were obtained by solid-state synthesis with stoichiometric proportions of reactants, namely NaF:VPO_4=1:1 feedstock for $NaVPO_4F$, and NaF:VPO_4=3:2 feedstock for $Na_3V_2(PO_4)_2F_3$. Barker's original 2003 reference described the thus-obtained $NaVPO_4F$ compound as tetragonal *I4/mmm*; but, it was mentioned in the same reference that the XRD pattern was "also in good accordance with the structural analysis of the related compound, $Na_3Al_2(PO_4)_3F_2$" [*sic*, the authors meant α-$Na_3Al_2(PO_4)_2F_3$] despite the obvious difference in stoichiometry, also *I4/mmm*, first described by Le Meins et al. in 1999, with *a*=6.206 Å and *c*=10.418 Å.[3a, 4] This allegedly *I4/mmm* $NaVPO_4F$ was reported with a high average discharge potential of 3.7 V (vs. hard carbon) and a specific capacity of 82 mAh g^{-1} (theoretical capacity should be 143 mAh g^{-1} if V^{3+}/V^{4+} is fully utilized), which might be comparable to the commercial cathode material $LiFePO_4$ (3.4 V vs. Li/Li^+ and theoretical capacity 170 mAh g^{-1}) of LIBs.[3a, 5] Since then, many groups have attempted to synthesize $NaVPO_4F$ to improve its electrochemical performance.

Zhuo et al. proposed a monoclinic Cr-doped $NaVPO_4F$ phase with space group C_2/c that provides 83.3 mAh g^{-1} reversible capacity, by solid-state synthesis.[6] However, thereupon they also mentioned that "The proposed structure is in good accordance with the structural analysis of the related compound, $Na_3Al_2(PO_4)_2F_3$" [*sic*, the authors meant $Na_3M_2(PO_4)_2F_3$ of

Le Meins' family].[4, 6] The work was then widely cited as $NaVPO_4F$, for example, Zhao et al. reported a phase transition of $NaVPO_4F$ from monoclinic to tetragonal structure during high temperature processing by sol-gel method.[7] Xu et al. synthesized tetragonal crystal $NaVPO_4F$ by hydrothermal method, and found that the obtained compound transformed into monoclinic phase after heating at 750 or 800 °C in Ar atmosphere.[8] Ruan et al. prepared graphene-modified tetragonal $NaVPO_4F$, and Jin et al. obtained monoclinic $NaVPO_4F$ nanofiber through electrospinning method.[9] Recently, Law and Balaya synthesized monoclinic $NaVPO_4F$ by a facile one-step soft template method which delivered high cycling stability.[10] Details of the crystal structures and phase transition between tetragonal and monoclinic $NaVPO_4F$ are confusing. Many of the works after Barker et al. and Zhuo et al. were based on the belief that monoclinic C_2/c and tetragonal I_4/mmm forms of $NaVPO_4F$ exist as single-phase compound after 1:1 stoichiometric solid-state synthesis.[3a, 6, 11]

Recently, Boivin et al. proposed a tavorite-type $NaVPO_4F$ by liquid-phase hydrothermal synthesis.[12] This structure is also monoclinic with space group of C_2/c. However, different from the previously stated structures with acclaimed (but puzzling) similarity to Le Meins family of $Na_3Al_2(PO_4)_2F_3$,[3a, 4, 6, 11] Boivin's structure is built up by VO_4F_2 octahedra chains connected to each other via PO_4 tetrahedra, similar to other tavorite-type compounds such as $LiVPO_4F$, $LiVPO_4OH$ and $HVPO_4OH$. For clarity, in this paper we will denote the

monoclinic structure pinned down by Boivin et al. as "tavorite-type", and the other monoclinic structure(s) as "non-tavorite monoclinic" $NaVPO_4F$. Note that while the crystal drawing of tavorite $NaVPO_4F$ was given by Boivin et al.,[12] the crystal drawing of non-tavorite C_2/c $NaVPO_4F$ was not provided,[6, 11] nor was that of tetragonal I_4/mmm $NaVPO_4F$.[3a] Thus, the non-tavorite C_2/c and the tetragonal I_4/mmm forms of $NaVPO_4F$ are mysterious to us.[3a, 6, 11]

Barker et al. demonstrated in 2006 that $Na_3V_2(PO_4)_2F_3$ can provide 115~120 mAh g^{-1} reversible capacity,[3b] and was initially solved to be tetragonal $P4_2/mnm$,[3b] belonging to Le Meins' family of $Na_3Al_2(PO_4)_2F_3$ polymorphs that include the tetragonal I_4/mmm α-$Na_3Al_2(PO_4)_2F_3$, and can undergo temperature-driven massive transformations within this family.[4] But its symmetry has been later revised and established as subtle orthorhombic (b/a = 1.002) space group *Amam* by Bianchini et al. by using a high angular resolution synchrotron diffraction, "preserving the global geometry of the $P4_2/mnm$ framework but showing a different distribution of sodium ions".[13] This crystal structure consists of pairs of corner-sharing VO_4F_2 octahedra, which are equatorially connected to PO_4 tetrahedra via O atoms. The doubt about the structural parallels between $NaVPO_4F$ and $Na_3Al_2(PO_4)_2F_3$ despite obvious stoichiometry difference was suggested by Sauvage et al.[14] Moreover, the clear difference in acclaimed lattice motifs in the two monoclinic $NaVPO_4F$ with same

materials stoichiometry and space group also fed our suspicion. Therefore, we initially seek to understand the formation mechanism and define the structure of $NaVPO_4F$.

Both powder and tablet samples were prepared via conventional solid-state synthesis method at temperatures from 550 to 750 °C. In situ X-ray diffraction (XRD) and thermogravimetric analysis/differential scanning calorimetry (TGA/DSC) measurement were employed to investigate the structural evolution details upon the heating process. The structural and compositional changes can be detected and quantified by recording spectra at a certain interval temperature. FT-IR, X-ray photoemission spectroscopy (XPS) and high resolution transmission electron microscopy (HRTEM) measurements were carried out to complement the XRD data. The structural and compositional evolution accompanied by detailed heating mechanisms during the electrochemical process was further evaluated.

Results and discussion

The XRD pattern with Rietveld refinement of the precursor phase (R_p=2.3%, R_{wp}=3.2%) is presented in Figure S1a. VPO_4 (ICDD PDF No. 01-086-1196) without any impurities is indeed formed according to Equation (M1) in methods. The ex situ XRD patterns of the tablet samples (NaF:VPO_4=1:1) treated at various temperatures (TS550, TS600, TS650, TS700 and

TS750) are shown in **Figure 1**a. XRD patterns are measured by mixing 5% silicon (ICDD PDF No. 01-089-2749) powder in these products to determine the exact composition of tablet samples. The results indicate that these samples are mainly composed of tetragonal $Na_3V_2(PO_4)_2F_3$ (ICDD PDF No. 01-089-8485) and VPO_4 below 650 °C. A new set of diffraction peaks of tablet samples can be indexed as the hexagonal crystalline $Na_3V_2(PO_4)_3$ (ICDD PDF No. 00-053-0018) above 600 °C, with a small amount of $(VO)_2P_2O_7$ (ICDD PDF No. 01-085-2281) and $Na_4P_2O_7$ (ICDD PDF No. 00-001-0356) byproducts. Upon further heating, a marked drop in the intensity of VPO_4 peaks and a gradual decline in $Na_3V_2(PO_4)_2F_3$ are also observed. Fig. 1b depicts the Rietveld refinement of TS600 on the basis of the XRD data, revealing that TS600 consists of $Na_3V_2(PO_4)_2F_3$ and VPO_4 with space group of $P4_2/mnm$ and *Cmcm* (R_p=3.9%, R_{wp}=5.5%), respectively. We are not able to confirm or deny the subtle orthorhombic space group *Amam* assignment to $Na_3V_2(PO_4)_2F_3$ by Bianchini et al. (*b/a* = 1.002) due to the resolution of our instrument.[13] Therefore, here we speculate that $NaVPO_4F$ cannot be synthesized by solid-state synthesis at any temperature, and $Na_3V_2(PO_4)_3$ is part of the reaction products between $Na_3V_2(PO_4)_2F_3$ and VPO_4. The schematic crystal structure of the tetragonal $P4_2/mnm$ / subtle orthorhombic (*b/a* = 1.002) *Amam* $Na_3V_2(PO_4)_2F_3$ and hexagonal $R\bar{3}c$ $Na_3V_2(PO_4)_3$ are shown in Figure 1c. Different from $Na_3V_2(PO_4)_2F_3$ with three dimensional structure of $V_2O_8F_3$ bi-octahedra bridged by PO_4 tetrahedra, $Na_3V_2(PO_4)_3$ is built by isolated VO_6 octahedra and PO_4 tetrahedra interlinked via

corners to establish the framework anion $[V_2(PO_4)_3]^{3-}$.[15] To further confirm our speculation, a powdery raw materials mixture ($NaF:VPO_4$=1:1) is also calcined at similar temperatures. XRD patterns of these powder samples (PS550, PS600, PS650, PS700, PS750 and PS800) are shown in Figure S1b. The graph shows that there has been a sharper decreasing trend in the intensities of $Na_3V_2(PO_4)_2F_3$ peaks until they disappeared altogether in PS800, suggesting that the tablet sample impeded volatilization of fluorine and reaction between $Na_3V_2(PO_4)_2F_3$ and VPO_4. To further confirm the synthetic products, samples with increasing ratio of feedstock NaF to VPO_4 (1.0:1 to 1.5:1) are calcined at 600 °C. As shown in Figure S1, there is a steady downward trend in the intensity of XRD peaks related to VPO_4 until it disappears eventually upon increasing NaF to VPO_4 ratio, demonstrating that only $Na_3V_2(PO_4)_2F_3$ could be synthesized in solid-state synthesis.

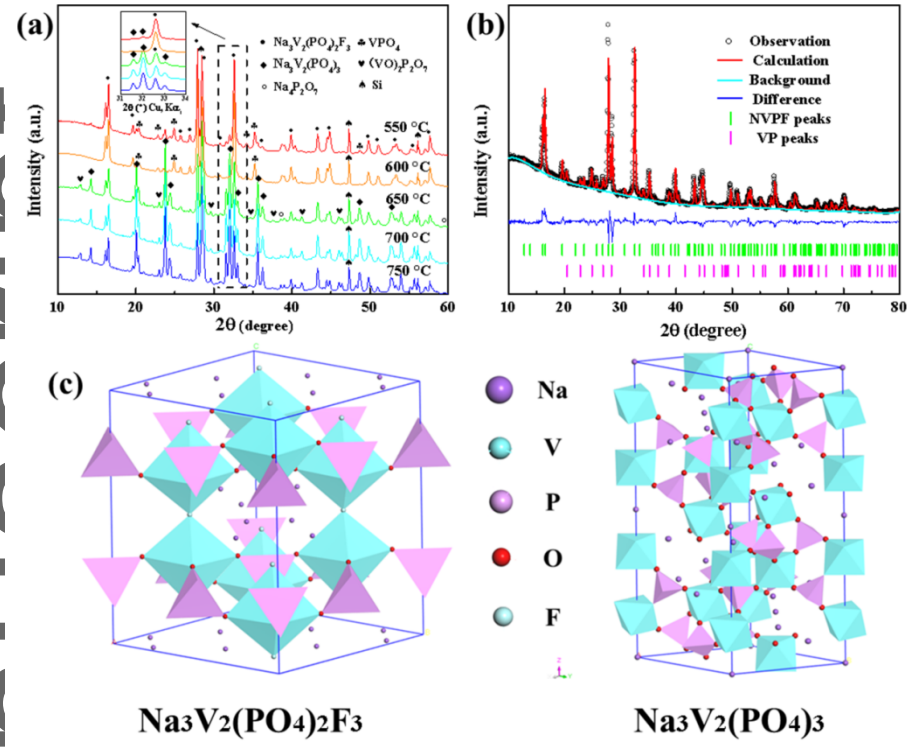

Figure 1 Crystal structure of $Na_3V_2(PO_4)_2F_3$ and $Na_3V_2(PO_4)_3$. (a) XRD patterns of the tablet samples calcined at 550-750 °C. (b) Rietveld refinement based on the XRD pattern of tablet sample calcined at 600 °C. Black circle, red line, cyan line and blue line represent the observed, calculated, background and difference patterns, respectively. The green and magenta tick marks correspond to the $Na_3V_2(PO_4)_2F_3$ and VPO_4 Bragg reflections, respectively. The abbreviation of NVPF and VP correspond to the $Na_3V_2(PO_4)_2F_3$ and VPO_4. (c) Schematic crystal structures of the tetragonal $P4_2/mnm$ / subtly orthorhombic (b/a = 1.002) *Amam* $Na_3V_2(PO_4)_2F_3$ and hexagonal $R\bar{3}c$ $Na_3V_2(PO_4)_3$.

To further understand crystal structure changes of the raw materials ($NaF:VPO_4$=1:1) from 25 to 950 °C, in situ XRD and TGA/DSC measurement are conducted (**Figure 2**). The heating process can be divided into four regimes by magenta lines in Figure 2: R1 for the preparation stage before solid-state reactions of raw materials below 400 °C, R2 for synthetic reaction of feedstock materials from 400 to 700 °C, R3 for chemical reaction between

$Na_3V_2(PO_4)_2F_3$ and VPO_4 from 700 to 850 °C and R4 for decomposition reaction of $Na_3V_2(PO_4)_3$ above 850 °C. For clarity, only the characteristic diffraction peak areas of the phases: (002) peak of NaF (ICDD PDF No. 01-070-2508); (111) and (112) peaks of VPO_4; (002) peak of $Na_3V_2(PO_4)_2F_3$; (113), (116) and (226) peaks of $Na_3V_2(PO_4)_3$; (113) peak of $(VO)_2P_2O_7$ and (005) peak of $Na_4P_2O_7$ are shown. Figure 2a displays the stacked in situ XRD patterns corresponding to TGA/DSC curves. Figure 2b shows the color-coded and temperature-resolved intensity plots. The reference color bar is located under each XRD peak/peak pair, respectively. In addition, specific proportions of different components during the compositional evolution by semi-quantitative calculation are displayed versus temperature in **Figure 3** and Table S1.

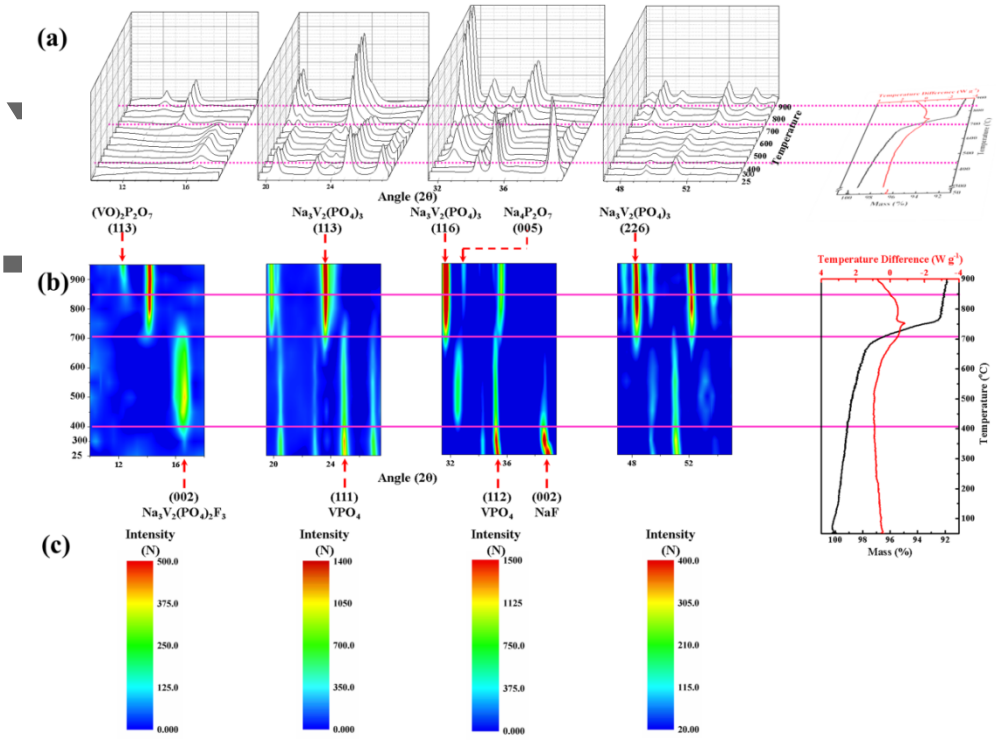

Figure 2 Structure and compositional evolution of raw materials upon heating. (a) Selected area and stacked in situ XRD patterns correspond to the TGA/DSC curves. (b) The color-coded, temperature-resolved, intensity distribution plots correspond to the TGA/DSC curves. (c) The reference color bar.

In R1 regime, with the temperature increasing up to 300 °C, all diffraction peaks of NaF and VPO_4 shift towards low angles. This phenomenon results from lattice expansion triggered by the atomic diffusion. When temperature increases up to 400 °C, intensity of NaF (002) peak weakens prominently while intensity of VPO_4 (111) and (112) peaks declines as well but much slower, indicating the reaction between NaF and VPO_4 occurs and the consumption rate of NaF is greater than VPO_4. The appearance of the new peak at 16.55° and

the residual peaks of unreacted VPO_4 affirms the tetragonal/orthorhombic $Na_3V_2(PO_4)_2F_3$ as a result of 3:2 reaction in a feedstock of 1:1 NaF and VPO_4.

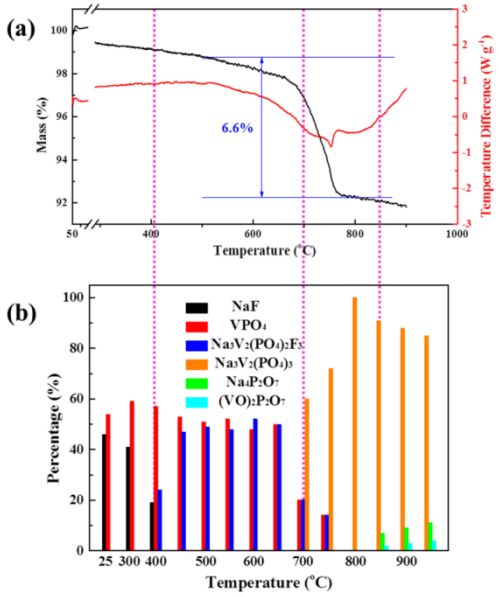

Figure 3 The specific compositional charges (atomic ratio) of raw materials upon heating. (a) The TGA/DSC curves of raw materials upon heating from 50 to 900 °C in Ar flow. (b) The corresponding specific compositional changes calculated by semi-quantitative calculation of in situ XRD patterns.

In R2 regime, the peak intensity of NaF keeps weakening until it disappears at 500 °C, while (002) peak of $Na_3V_2(PO_4)_2F_3$ continues to increase, indicating the synthetic reaction keeps proceeding until NaF runs out. It should be noted that the ratio of $Na_3V_2(PO_4)_2F_3$ and VPO_4 remains 1:1 until both of them exhausted at 800 °C, which matches the expected proportion after 3:2 synthetic reaction of $Na_3V_2(PO_4)_2F_3$, confirming the reaction product is $Na_3V_2(PO_4)_2F_3$ instead of tetragonal $NaVPO_4F$.

In R3 regime, from both stacked linear diffraction pattern and color-coded intensity plots in Figure 2, it is clear that the peak intensities of both $Na_3V_2(PO_4)_2F_3$ and VPO_4 significantly decline when temperature rises to 700 °C, whereas another series of new and strong peaks emerge, whose peak positions are nearly the same as the proposed monoclinic $NaVPO_4F$ phase reported by many previous works.[6-7, 9b, 11, 16] To further investigate the new crystal structure, the TGA/DSC measurement corresponding to *in situ* XRD was employed. As shown in Figure 2 and 3, there are a remarkable weight loss (~6.6%) and a strong endothermic peak from 650 to 800 °C corresponding to the generation of the new peaks. This weight loss precludes the possibility of $Na_3V_2(PO_4)_2F_3 + VPO_4 = 3NaVPO_4F$. After careful comparison, these new peaks can be attributed to hexagonal $Na_3V_2(PO_4)_3$ (space group $R\bar{3}c$.), with weight loss attributed to volatile VF_3 (gas). The ~6.6% weight loss is less than the theoretical proportion of VF_3 (~17.5%) because part of the VF_3 is obstructed by the coating layer of amorphous carbon.[17] Therefore, tetragonal I_4/mmm and non-tavorite monoclinic C_2/c $NaVPO_4F$ may not exist. They might instead be tetragonal $P4_2/mnm$ / subtle orthorhombic (b/a = 1.002) *Amam* $Na_3V_2(PO_4)_2F_3$ and $R\bar{3}c$ $Na_3V_2(PO_4)_3$, respectively, shown in Figure 1c, depending on the thermal treatment temperature. Because of the loss of VF_3, there can be no formation of or phase transition to non-tavorite monoclinic C_2/c phase $NaVPO_4F$ at still higher temperatures. Besides, pure rhombohedral $Na_3V_2(PO_4)_3$ are detected after complete chemical reaction at 800 °C.

In R4, a progressive increase of several new peak intensities is observed at 850 °C, satisfying the mechanism of Equation (3) occurring at high temperature.[18] These new peaks can be attributed to the $(VO)_2P_2O_7$ (113) reflection and $Na_4P_2O_7$ (005) peak after rigorous analysis. Therefore, rhombohedral $Na_3V_2(PO_4)_3$ cannot sustain temperature above 800 °C and will decompose to $(VO)_2P_2O_7$, $Na_4P_2O_7$ and maybe other amorphous products (AP) that we have not clarified yet.[19] Due to tableting of raw materials and gaseous reaction product, chemical reaction between $Na_3V_2(PO_4)_2F_3$ and VPO_4 is far from completed in TS750. Moreover, the chemical reaction between $Na_3V_2(PO_4)_2F_3$ and VPO_4 and decomposition reaction of $Na_3V_2(PO_4)_3$ are simultaneously occurring at 650 °C, ascribed to the long heat preservation (8 h) for powder samples. To summarize, the structural and compositional evolution in synthesis process of raw materials can be described as follows:

$$3NaF + 3VPO_4 \rightarrow Na_3V_2(PO_4)_2F_3 + VPO_4 \quad \text{(up to 500 °C)} \quad (1)$$

$$Na_3V_2(PO_4)_2F_3 + VPO_4 \rightarrow Na_3V_2(PO_4)_3 + VF_3\uparrow \quad \text{(600 to 800 °C)} \quad (2)$$

$$2Na_3V_2(PO_4)_3 \rightarrow 2(VO)_2P_2O_7 + Na_4P_2O_7 + AP \quad \text{(above 800 °C)} \quad (3)$$

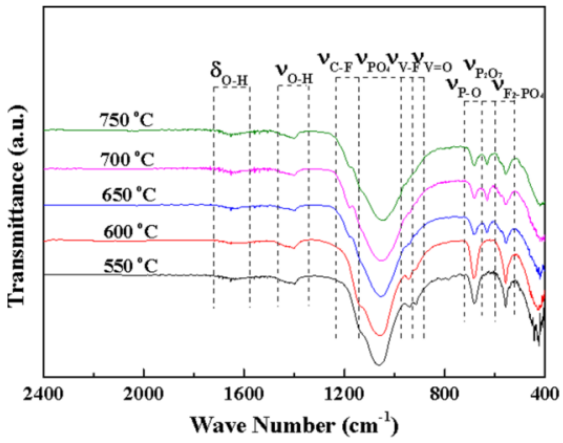

Figure 4 FT-IR spectra of tablet samples calcined at 550 - 750 °C.

Figure 4 shows FT-IR spectra between 2400 cm^{-1} to 400 cm^{-1} for as-synthesized products. The weak bands at 1650 cm^{-1} and 1398 cm^{-1} can be ascribed to O-H bending and O-H vibration of C-OH groups.[20] When the temperature rises, these two bands become weaker in powder samples (Figure S2), but no such change occurs in the tablet samples. This phenomenon indicates tablet hinders the release of gases and the breakdown of C-OH groups. Strong broad band at 1060 cm^{-1} can be attributed to asymmetric stretching of PO_4^{3-} tetrahedron.[21] The relative strength of the bands of absorbance of C-F bond at 1178 cm^{-1}, stretching vibration of V-F bond at 944 cm^{-1}, symmetric stretching mode of P-O bond at 673 cm^{-1}, vibration of $P_2O_7^{4-}$ unit at 602 cm^{-1} and asymmetric bending vibration $\nu(F_2)$ of PO_4^{3-} at 556 cm^{-1} varies with the rising temperature.[21-22] Stretching vibration of V-F bond (944 cm^{-1}) becomes weaker until it disappeared, whereas absorbance of C-F bond (1178 cm^{-1}) becomes slightly stronger. It indicates Equation (2) reaction is sustained and part of evaporable

fluoride is captured by carbon coating layer. Furthermore, symmetric stretching of P-O bond (673 cm^{-1}) and asymmetric bending vibration $\nu(F_2)$ of PO_4^{3-} (556 cm^{-1}) keep lessening, whereas vibration of $P_2O_7^{4-}$ unit (602 cm^{-1}) intensifies along with the rising temperature above 650 °C. It means the $V_2O_8F_3$ bi-octahedra in $Na_3V_2(PO_4)_2F_3$ transfers to isolated VO_6 octahedra in $Na_3V_2(PO_4)_3$ and the reaction product $Na_3V_2(PO_4)_3$ further decompose as $Na_4P_2O_7$, $(VO)_2P_2O_7$ and other AP. The much weaker intensity of bands at 944 cm^{-1} and 556 cm^{-1} in powder samples obtained at 800 °C (Figure S2) also demonstrates that compact tablet impedes the fluorine from fleeing the crystal lattice of $Na_3V_2(PO_4)_2F_3$. Overall, the peak shift and intensity in in-situ and ex-situ XRD patterns and the varying strength and position for bands in FT-IR spectra confirm that V-F bonds rupture in crystal, fluorine run away from the $Na_3V_2(PO_4)_2F_3$ and part of PO_4^{3-} unit transfer into $P_2O_7^{4-}$ group, affirming that feedstock materials undergo three reactions Equation (1), (2) and (3) upon heating.

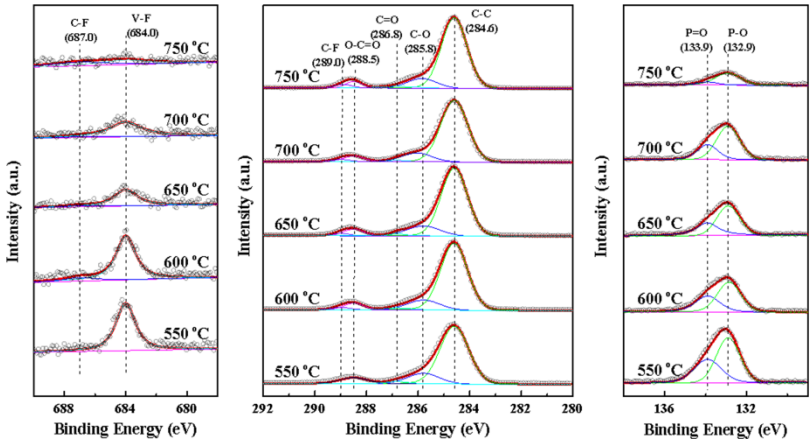

Figure 5 XPS spectra of F 1*s*, C 1*s* and P 2*p* for tablet samples calcined at 550 - 750 °C.

X-ray photoelectron spectroscopy (XPS) analysis of tablet samples is shown in **Figure 5**. In the F 1s spectra, two components of F-C bond at 687.0 eV and F-V bond at 684.0 eV are observed. The intensity of F-V bond is gradually and significantly reduced, and F-C bond increased much slower as resultant temperature increases, illustrating that the group related to F-V bond is tapered off and only part of fluorine has been captured by the coating carbon layer.[23] The C 1s region for tablet samples can be deconvoluted into five Gaussian peaks: C-C at 284.6 eV, C-O at 285.8 eV, C=O at 286.8 eV, O-C=O at 288.5 eV and C-F at 289.0 eV.[20b, 23a, 24] The same trend as F-C bond in F 1s region confirms the speculation about the evolution of groups related to fluorine analyzed by in situ XRD and FT-IR measurement. The P 2p spectra are characterized by a broadened band which can be decomposed in two different components at 133.9 eV for P=O bond and 132.9 eV for P-O bond. The intensity of the broadened band suddenly weakens after 700 °C, in good agreement with the decomposition mechanism of $Na_3V_2(PO_4)_3$ at high temperature shown in Equation (3).

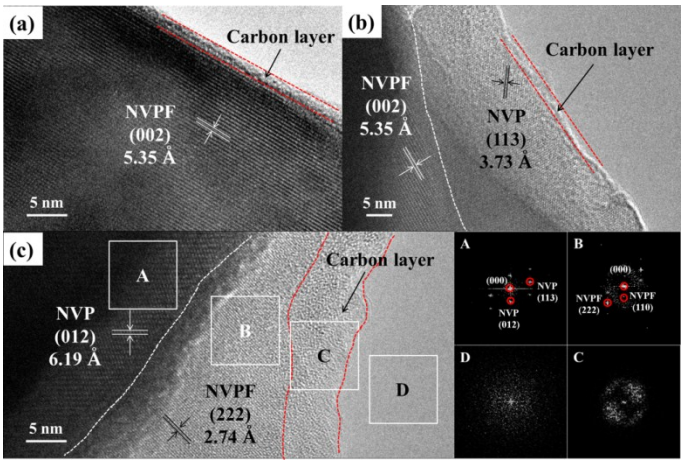

Figure 6 HRTEM images of tablet samples calcined at (a) 550, (b) 650 and (c) 750 ºC and FFT pictures correspond to the selected areas. The abbreviation of NVPF and NVP correspond to the $Na_3V_2(PO_4)_2F_3$ and $Na_3V_2(PO_4)_3$.

The characteristic Raman peaks are located at 1327, 1587 and 2654 cm^{-1} (Figure S5a), corresponding to the D, G and 2D bands of carbonaceous materials, respectively. It has been reported that the relative intensity ratio of D and G bands (ID/IG) indicates degree of crystallinity in various carbon materials.[25] The ID/IG of each tablet samples is larger than 1, indicating the amorphous nature of carbon. The amount of carbon is estimated to be approximately 6% in the tablet samples (Figure S3b) from the weight loss in air flow. The morphology of tablet samples is exhibited in Figure S3. It is clear that all compounds composed of agglomerated nanoparticles, with secondary particle sizes mainly distributed around 1.5 μm. The nanoparticles clinging to secondary particles surface of tablet samples calcined above 600 ºC might be ascribed to chemical reaction between $Na_3V_2(PO_4)_2F_3$ and VPO_4 and decomposition process of $Na_3V_2(PO_4)_3$. In contrast to stable P element, the amount of F element decline steadily after 600 ºC (Figure S4), in good agreement with Equation (2). High resolution transmission electron microscopy (HRTEM) images confirm the composite structure of crystalline particles and amorphous carbon. As shown in **Figure 6**, all sample surfaces are well coated by amorphous carbon layer thinner than 5 nm, especially in TS550 and TS650, revealing that the fluorine escaped from $Na_3V_2(PO_4)_2F_3$ lattice could be scavenged by the carbon layers. The lattice fringe of 5.35 Å can be observed inside the

particles in TS550, consistent with the interplanar spacing of (002) plane of $Na_3V_2(PO_4)_2F_3$, which demonstrate that TS550 is mainly composed of $Na_3V_2(PO_4)_2F_3$ particles. As for TS650, the crystallization region is obviously divided into two parts: a highly crystalline layered structure with a layer distance of 5.35 Å corresponding to interplanar spacing of (002) plane of $Na_3V_2(PO_4)_2F_3$ on the left side, and another crystalline particle with fringe spacing of 3.73 Å consistent with (002) plane of $Na_3V_2(PO_4)_3$ on right side. Four divided parts of the multicomponent TS750 are shown in Figure 6c. On the basis of relevant fast Fourier transformation (FFT) images, crystal in part A can be ascribed to the newly formed $Na_3V_2(PO_4)_3$ particles; crystal in part B can be attributed to the residual $Na_3V_2(PO_4)_2F_3$ particles; amorphous layer in part C can be established as the coating carbon layer, and empty region in part D is gap of the TEM micro grid copper network. These results have recorded the process of constant loss of $Na_3V_2(PO_4)_2F_3$ and new generation of $Na_3V_2(PO_4)_3$ crystals, consistent with Equation (1) and (2).

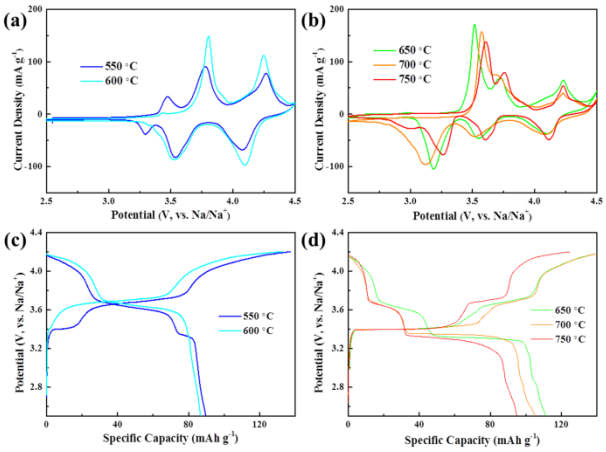

Figure 7 CV and the first cycle charge and discharge curves of tablet samples calcined at (a) (c) 550 - 600 °C, (b) (d) 650 - 750 °C.

CR2016 coin cells with Na metal anode were assembled to investigate the detailed electrochemical performance of tablet and powder samples. **Figure 7** shows the CV curves of samples tested in potential range of 2.5~4.5 V (vs. Na/Na^+) at a scan rate of 0.1 $mV \cdot s^{-1}$. When the temperature is elevated up to 550 °C and 600 °C, the samples exhibit two couples of redox peaks (~4.3 V/4.1 V and ~3.8 V/3.6 V vs. Na/Na^+) which belong to $Na_3V_2(PO_4)_2F_3$, and a couple of small redox peaks around 3.4 V/3.3 V (vs. Na/Na^+) is attributed to $Na_3V_2(PO_4)_3$ for TS550. It demonstrates that the main active materials calcined below 650 °C is the well-established $Na_3V_2(PO_4)_2F_3$. However, a couple of strong redox peaks of ~3.4 V/3.3 V (vs. Na/Na^+) which belong to $Na_3V_2(PO_4)_3$ arise when temperature increased above 600 °C. Besides, another small and broad redox peaks around 2.9 V (vs. Na/Na^+) are observed, belonging to the decomposition product of $Na_3V_2(PO_4)_3$.[18] The redox peaks of

$Na_3V_2(PO_4)_2F_3$ (~4.3 V/4.1 V and ~3.8 V/3.6 V vs. Na/Na^+) and $Na_3V_2(PO_4)_3$ (~3.4 V/3.3 V vs. Na/Na^+) become weaker during elevated sintering temperature above 650 °C, whereas the small redox peaks around 2.9 V (vs. Na/Na^+) become even larger.[18] The corresponding charge/discharge curves at 0.1 C-rate (0.1 C means full charge/discharge in 10 h) are presented in Figure 7c and d. The initial charge/discharge curves of the test cells deliver an initial discharge capacity of 89.7, 86.7, 111.4, 105.3 and 94.9 mA h g^{-1} of TS550, TS600, TS650, TS700 and TS750. The specific charge and discharge potential plateaus (3.5 V/3.3 V vs. Na/Na^+) capacity of $Na_3V_2(PO_4)_3$ increases at first and then decreases at temperatures above 650 °C. These results indicate that chemical reaction between $Na_3V_2(PO_4)_2F_3$ and VPO_4 and decomposition reaction of $Na_3V_2(PO_4)_3$ occur at same time when the temperature increases up to 650 °C. The charge and discharge curves of powder samples (Figure S6) show there is a diminishing trend in plateaus of $Na_3V_2(PO_4)_2F_3$. The difference of charge and discharge curves between tablet and powder samples illustrates that compacted tablet blocks the continuous reaction between $Na_3V_2(PO_4)_2F_3$ and VPO_4 and hinder the fleeing of fluorine.

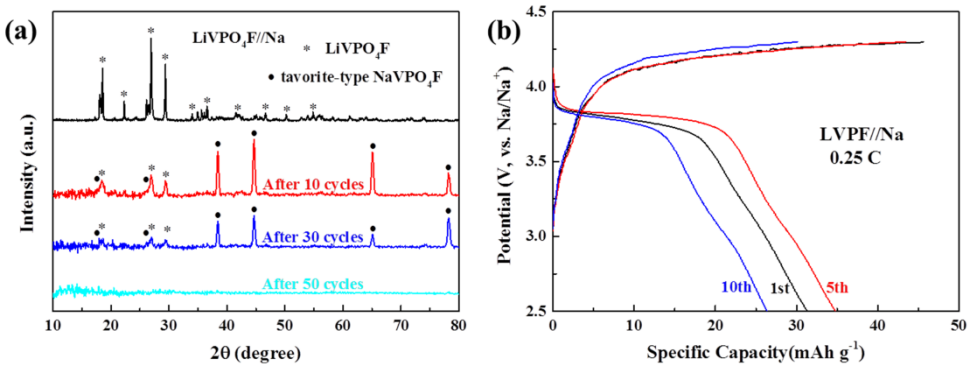

Figure 8 (a) XRD patterns of $LiVPO_4F$ and the ion exchange compound after 10, 30 and 50 cycles in a sodium cell; (b) The 1st , 5th and 10th charge and discharge curves of $LiVPO_4F$ in sodium cell with a potential window of 2.5–4.3 V (vs. Na/Na^+).

Based on our experience, with 1:1 $NaF:VPO_4$ feedstock and solid-state synthesis one cannot get single-phase $NaVPO_4F$ compound at any temperature. Instead, one gets two-phase mixture of $Na_3V_2(PO_4)_2F_3$+VPO_4 up to 500°C. The resulting tetragonal *P4₂/mnm* / subtle orthorhombic (*b/a* = 1.002) *Amam* $Na_3V_2(PO_4)_2F_3$ may be easily mistaken to be tetragonal *I4/mmm*.[3a] And then from 600 to 800 °C, $Na_3V_2(PO_4)_2F_3$+VPO_4→$Na_3V_2(PO_4)_3$+VF_3↑. The degree of VF_3 volatilization depend on the temperature exposure and details of pelletization, however some vaporization of VF_3 and mass loss is unavoidable after 650 °C. Since $Na_3V_2(PO_4)_3$ is rhombohedral $R\bar{3}c$, it may also be easily mistaken to be non-tavorite monoclinic *C2/c* $NaVPO_4F$.[6, 11] Based on Barker et al. and Zhuo et al.,[3a, 6] many researchers have quoted tetragonal *I4/mmm* and non-tavorite monoclinic *C2/c* $NaVPO_4F$ from solid-state synthesis, for example Zhao et al. reported a gradual phase transition of $NaVPO_4F$ from

monoclinic at 700 °C to tetragonal at 750 °C,[7] however we believe these assignments of single-phase $NaVPO_4F$ compound may often be mistaken.

Since we have not obtained $NaVPO_4F$ with solid-state synthesis, we would like to form $NaVPO_4F$ by another method, liquid-aided electrochemical ion exchange. We perform Li→Na ion exchange on $LiVPO_4F$, by introducing $LiVPO_4F$ as cathode to cycle in a sodium half-cell to form $NaVPO_4F$ electrochemically for comparison.[17, 26] As shown in **Figure 8**, the XRD patterns of $LiVPO_4F$ and the ion exchanged compound after 10, 30 and 50 cycles are well observed. After 10 cycles' electrochemical ion exchange process, Na ions are expected to be the cations reinserted into VPO_4F framework due to preponderant Na ion concentration in sodium half-cell. The crystal structure has changed dramatically after 10 cycles which can be ascribed to the formation of $NaVPO_4F$. However, this new structure of $NaVPO_4F$ by liquid-phase method is far different from the hypothetical tetragonal I_4/mmm and non-tavorite C_2/c $NaVPO_4F$ of previous reports (in the sense that although no explicit atomic coordinates were given and of a different stoichiometry, they were all acclaimed to be as similar to Le Meins' family).[3a, 4, 6] These liquid-phase $NaVPO_4F$ belongs to the Tavorite family instead.[3a, 6-8, 9b, 12, 16, 27] Furthermore, a unique and distinct charge/discharge plateaus at ~3.9 V (vs. Na/Na^+) is detected in charge and discharge curves (Figure 8b), which is different from the tetragonal (4.1 V and 3.6 V vs. Na/Na^+) and non-tavorite monoclinic

"$NaVPO_4F$" (3.4 V vs. Na/Na),[3a, 6-8, 9b, 16, 27] now strongly suspected to be multi-phase mixtures of Le Meins' $Na_3V_2(PO_4)_2F_3$, VPO_4 and $Na_3V_2(PO_4)_3$. Therefore, we would like to suggest that the tetragonal $NaVPO_4F$ and non-tavorite monoclinic $NaVPO_4F$ are probably wrong assignments in previous cognitions,[3a, 6] while tavorite-type $NaVPO_4F$ (by electrochemical ion exchange) and tetragonal *P4₂/mnm* / subtly orthorhombic (*b/a* = 1.002) *Amam* $Na_3V_2(PO_4)_2F_3$ (by solid-state synthesis) can truly be formed.

Conclusions

Careful analysis of in-situ XRD during the solid-state synthesis of raw materials (NaF and VPO_4 mixture with proportion of 1:1) provides insight into the reaction and formation mechanism of tetragonal *P4₂/mnm* / subtly orthorhombic (*b/a* = 1.002) *Amam* $Na_3V_2(PO_4)_2F_3$ of Le Meins' family, but not $NaVPO_4F$. 3:2 reaction of NaF:VPO_4 into $Na_3V_2(PO_4)_2F_3$ occurred first at 400 °C; 1:1 chemical reaction between $Na_3V_2(PO_4)_2F_3$:VPO_4 was observed at 700 °C, but instead of forming $NaVPO_4F$ as one might expect, due to volatilization of VF_3, $Na_3V_2(PO_4)_3$ was formed; decomposition of $Na_3V_2(PO_4)_3$ was discovered at 850 °C. The tablet and powder samples calcined at various temperatures convincingly demonstrate these three reactions, in addition to the different reaction temperatures with longtime insulation. The electrochemical ion exchange of $LiVPO_4F$ provides the tavorite-type $NaVPO_4F$, far from

the hypothetical tetragonal and non-tavorite monoclinic $NaVPO_4F$ structures reported previously, or Le Meins' family $Na_3V_2(PO_4)_2F_3$. The results presented here clarify the misunderstandings and illustrate that tetragonal $NaVPO_4F$ (space group I_4/mmm) probably does not exist. Moreover, due to the major weight loss, non-tavorite monoclinic $NaVPO_4F$ might be misleading. These structures might be multi-phase mixtures of Le Meins' $Na_3V_2(PO_4)_2F_3$, unreacted VPO_4 andhexagonal $Na_3V_2(PO_4)_3$ instead. The understanding gained about the formation mechanism upon heating process of 1:1 $NaF:VPO_4$ raw materials we proposed may help us avoid future mislabeling of fluorophosphate SIB cathode materials.

Methods

Materials preparation

The active materials calcined at different temperature were prepared by a traditional two-step carbothermal reduction route. V_2O_5 and $NH_4H_2PO_4$ with a stoichiometric amount was firstly ball milled with acetylene black (20% excess) in 400 rpm for 6 h to get a uniform particles distribution. The mixture was calcined at 750 °C for 8 h in argon (Ar) atmosphere to obtain VPO_4. The active materials were prepared by mixing and tablet or not with proportion (1:1) of the intermediate VPO_4 and NaF, then sintered at 550, 600, 650, 700 and 750 °C under Ar flow for 8 h, respectively. The first step incorporation reaction may be summarized as:

$$V_2O_5 + 2NH_4H_2PO_4 + 2C \rightarrow 2VPO_4 + 2NH_3 + 3H_2O + 2CO \quad (M1)$$

The unexhausted acetylene black was left as carbon coating on the surface of the active materials in the final product.

Characterization

In situ and ex situ XRD measurement was performed to characterize the structural and compositional evolution upon heating by using an X'pert Pro (PANalytical Ltd., Holland) with Cu Kα radiation (λ=1.5406 Å). Characteristic weight loss and thermodynamic heat energy transmission of the second step mixture precursor were measured by TGA/DSC analyses using a Mettler Toledo (TGA/DSC 1) thermoanalyzer. The measurement was conducted from room temperature to 900 °C at a heating rate of 10 °C min^{-1}. The IR spectra were obtained by FTIR Spectrometer (Nicolet, iS10, USA) under transmission mode based on the KBr pellet method in the range of 400-4000 cm-1. XPS was collected by using a monochromatic Al Ka (1486.6 eV) radiation. Raman spectra were obtained on a HORIBA JOBIN YVON micro-Raman spectrometer. The particle morphology of the active materials (heat-treatment at 550~750 °C, at an interval of 50 °C, in the second step) was observed by field emission scanning electron microscopy (FE-SEM Quanta 250FEG, FEI, USA).

Transmission electron microscopy (TEM, FEI TITAN G2, USA) was employed to characterize the morphology as well as the evolution of raw materials upon heating.

Electrochemical measurement

The electrochemical performance was carried out with 2016 coin cells assembled in glove box filled with high-purity argon gas. In the sodium half cells, the 70% active material, 20% conducting carbon (super P) and 10% binder (PVDF) were used as the cathode, a microporous polymer (Celgard 2500) as separator, the sodium metal as the anode, and 1 M solution of $NaClO_4$ in EC-DMC (50:50) as the electrolyte. The mass loading of active material in each coin cell is typically 1.0~1.5 mg cm^{-2}, and the electrode footprint area is 2.01 cm^2. The galvanostatic charge/discharge at the range of 2.5 to 4.2 V vs. Na/Na^+ was measured on a CT2001A Land Battery Testing System, while the cyclic voltammetry (CV) was performed on a Versatile Multichannel Galvanostat 2/Z (VMP2, Princeton Applied Research).

Supporting Information

Supporting Information is available from the Wiley Online Library or from the author.

Acknowledgements

This work is financially supported by the National Natural Science Foundation of China (Grant No. 21503158), the National Natural Science Foundation of China (Grant No. 51772240), the Key Research and Development Plan of Shaanxi Province (China, 2017ZDCXL-GY-08-02), the Natural Science Foundation of Shaanxi Province (China, Grant No. 2014JQ2-2007), the 111 Project（B14040）and the Fundamental Research Funds for the Central Universities of China (Grant No. xjj2014044).

The SEM/TEM work was done at the International Center for Dielectric Research (ICDR), Xi'an Jiaotong University, Xi'an, China; we also thank Lu Lu for her help in using TEM.

References

[1] a) E. C. Evarts, *Nature* **2015**, 526, S93; b) H. Hongshuai, S. Lidong, Z. Yan, Z. Guoqiang, C. Jun, J. Xiaobo, *Adv. Sci.* **2017**, 4, 1600243; c) H. Hou, C. E. Banks, M. Jing, Y. Zhang, X. Ji, *Adv. Mater.* **2015**, 27, 7861.

[2] Q. Ni, Y. Bai, F. Wu, C. Wu, *Adv. Sci.* **2017**, 4, 1600275.

[3] a) J. Barker, M. Y. Saidi, J. L. Swoyer, *Electrochem. Solid-State Lett.* **2003**, 6, A1; b) J. Barker, R. K. B. Gover, P. Burns, A. J. Bryan, *Electrochem. Solid-State Lett.* **2006**, 9, A190.

[4] J. M. Le Meins, M. P. Crosnier-Lopez, A. Hemon-Ribaud, G. Courbion, *J. Solid State Chem.* **1999**, 148, 260.

[5] C. Delacourt, L. Laffont, R. Bouchet, C. Wurm, J. B. Leriche, M. Morcrette, J. M. Tarascon, C. Masquelier, *J. Electrochem. Soc.* **2005**, 152, A913.

[6] H. Zhuo, X. Wang, A. Tang, Z. Liu, S. Gamboa, P. J. Sebastian, *J. Power Sources* **2006**, 160, 698.

[7] J. Zhao, J. He, X. Ding, J. Zhou, Y. o. Ma, S. Wu, R. Huang, *J. Power Sources* **2010**, 195, 6854.

[8] M. Xu, C.-J. Cheng, Q.-Q. Sun, S.-J. Bao, Y.-B. Niu, H. He, Y. Li, J. Song, *RSC Adv.* **2015**, 5, 40065.

[9] a) Y.-L. Ruan, K. Wang, S.-D. Song, X. Han, B.-W. Cheng, *Electrochim. Acta* **2015**, 160, 330; b) T. Jin, Y. C. Liu, Y. Li, K. Z. Cao, X. J. Wang, L. F. Jiao, *Adv. Energy Mater.* **2017**, 7, 1700087.

[10] M. Law, P. Balaya, *Energy Storage Materials* **2018**, 10, 102.

[11] Z.-m. Liu, X.-y. Wang, Y. Wang, A.-p. Tang, S.-y. Yang, L.-f. He, *Trans. Nonferrous Met. Soc. China* **2008**, 18, 346.

[12] E. Boivin, J. N. Chotard, T. Bamine, D. Carlier, P. Serras, V. Palomares, T. Rojo, A. Iadecola, L. Dupont, L. Bourgeois, F. Fauth, C. Masquelier, L. Croguennec, *J. Mater. Chem. A* **2017**, 5, 25044.

[13] a) M. Bianchini, F. Fauth, N. Brisset, F. Weill, E. Suard, C. Masquelier, L. Croguennec, *Chem. Mater.* **2015**, 27, 3009; b) I. Spanopoulos, W. Ke, C. C. Stoumpos, E. C. Schueller, O. Y. Kontsevoi, R. Seshadri, M. G. Kanatzidis, *J. Am. Chem. Soc.* **2018**, 140, 5728; c) A. L. Balch, K. Winkler, *Chem. Rev.* **2016**, 116, 3812.

[14] F. Sauvage, E. Quarez, J. M. Tarascon, E. Baudrin, *Solid State Sci.* **2006**, 8, 1215.

[15] a) S. Li, Y. Dong, L. Xu, X. Xu, L. He, L. Mai, *Adv. Mater.* **2014**, 26, 3545; b) J.-N. Chotard, G. Rousse, R. David, O. Mentré, M. Courty, C. Masquelier, *Chem. Mater.* **2015**, 27, 5982; c) Y. Fang, L. Xiao, X. Ai, Y. Cao, H. Yang, *Adv. Mater.* **2015**, 27, 5895; d) K. Saravanan, C. W. Mason, A. Rudola, K. H. Wong, P. Balaya, *Adv. Energy Mater.* **2013**, 3, 444.

[16] Y. Lu, S. Zhang, Y. Li, L. Xue, G. Xu, X. Zhang, *J. Power Sources* **2014**, 247, 770.

[17] J.-M. Ateba Mba, C. Masquelier, E. Suard, L. Croguennec, *Chem. Mater.* **2012**, 24, 1223.

[18] W. Song, X. Ji, Y. Yao, H. Zhu, Q. Chen, Q. Sun, C. E. Banks, *PCCP* **2014**, 16, 3055.

[19] a) J. Meng, H. Guo, C. Niu, Y. Zhao, L. Xu, Q. Li, L. Mai, *Joule* **2017**, 1, 522; b) A. Wang, S. Kadam, H. Li, S. Shi, Y. Qi, *npj Comput. Mater.* **2018**, 4, 15.

[20] a) A. Paolella, G. Bertoni, E. Dilena, S. Marras, A. Ansaldo, L. Manna, C. George, *Nano Lett.* **2014**, 14, 1477; b) M. J. Aragón, P. Lavela, G. F. Ortiz, J. L. Tirado, *ChemElectroChem* **2015**, 2, 995.

[21] Y. Qi, L. Mu, J. Zhao, Y.-S. Hu, H. Liu, S. Dai, *Angew. Chem. Int. Ed.* **2015**, 54, 9911.

[22] a) M. E. Holtz, Y. Yu, D. Gunceler, J. Gao, R. Sundararaman, K. A. Schwarz, T. A. Arias, H. D. Abruña, D. A. Muller, *Nano Lett.* **2014**, 14, 1453; b) A. Ait Salah, P. Jozwiak, K. Zaghib, J. Garbarczyk, F. Gendron, A. Mauger, C. M. Julien, *Spectrochim. Acta, Part A* **2006**, 65, 1007; c) N. Suzuki, W. D. Richards, Y. Wang, L. J. Miara, J. C. Kim, I.-S. Jung, T. Tsujimura, G. Ceder, *Chem. Mater.* **2018**, 30, 2236; d) B. L. Corso, I. Perez, T. Sheps, P. C. Sims, O. T. Gül, P. G. Collins, *Nano Lett.* **2014**, 14, 1329.

[23] a) R. Zhang, X. Chen, X. Shen, X.-Q. Zhang, X.-R. Chen, X.-B. Cheng, C. Yan, C.-Z. Zhao, Q. Zhang, *Joule* **2018**, 2, 764; b) J. Zhang, W. Lv, D. Zheng, Q. Liang, D.-W. Wang, F. Kang, Q.-H. Yang, *Adv. Energy Mater.* **2018**, 8, 1702395.

[24] J. Ren, Y. Zhang, W. Bai, X. Chen, Z. Zhang, X. Fang, W. Weng, Y. Wang, H. Peng, *Angew. Chem. Int. Ed. Engl.* **2014**, 53, 7864.

[25] Y. H. Jung, C. H. Lim, D. K. Kim, *J. Mater. Chem. A* **2013**, 1, 11350.

[26] a) X. Sun, Y. Xu, M. Jia, P. Ding, Y. Liu, K. Chen, *J. Mater. Chem. A* **2013**, 1, 2501; b) C. Yang, X. Ji, X. Fan, T. Gao, L. Suo, F. Wang, W. Sun, J. Chen, L. Chen, F. Han, L. Miao, K. Xu, K. Gerasopoulos, C. Wang, *Adv. Mater.* **2017**, 29.

[27] a) C. Chang, Y. Li, W. He, G. Li, W. Guo, P. Zhu, M. Yao, J. Feng, *Mater. Lett.* **2017**, 209, 82; b) M. Law, P. Balaya, *Energy Storage Materials* **2018**, 10, 102.

Graphical abstract :

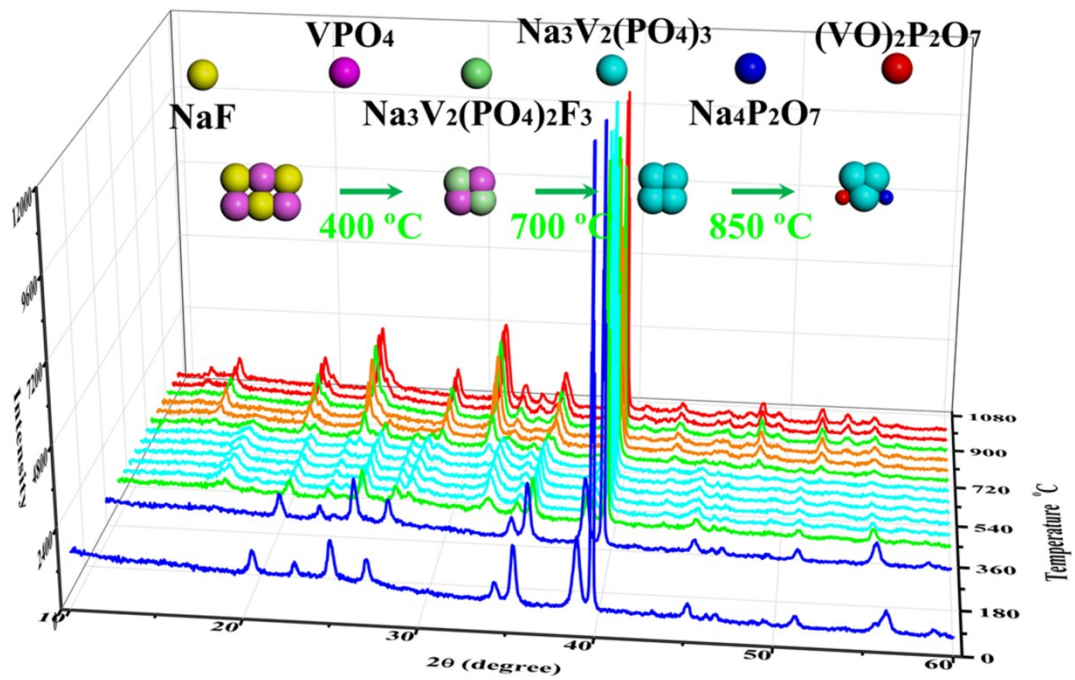

Short summary:

Systematic investigation of the mechanism underlying structural and compositional evolution of solid-state synthesis ($NaF:VPO_4$=1:1) process is determined by in-situ and ex-situ XRD and electrochemical measurements. After the careful analysis, we speculate that the perceptions of tetragonal and non-tavorite monoclinic $NaVPO_4F$ are incorrect, and only tavorite-type $NaVPO_4F$ and tetragonal/orthorhombic $Na_3V_2(PO_4)_2F_3$ can be formed.